exhibits a strength maximum. The reduction in fracture toughness above 1550°C could result from two factors. For the dense as-hot-pressed material, the high gas pressures generated internally during the higher temperature anneals could nucleate some microcracks and weaken the material by providing low energy crack paths. This may also have occurred to a lesser extent in the material hot-pressed at 1300°C if annealing at the higher temperatures caused the material to sinter up before all the impurities had escaped through the connected porosity. In fact, the densities of this material annealed at 1750°C were slightly lower than that for material annealed at 1550°C. In addition, the fracture toughness-grain size effect reported for cold-pressed and sintered material [3] could be taking effect as the grain size begins to increase rapidly. This effect (amounting to a 15% decrease in K_{IC} between grain sizes of 4 and 20 μm) is not sufficient to account for the entire decrease in fracture toughness above 1550°C, hence, both effects probably contribute. The variability of the above effects coupled with the location of the occasional large pore on the crack path probably accounts for the increased scatter in Fig. 3 above 1600°.

The strength after annealing of material hot-pressed at 1300° is consistently higher than that for material exhibiting pore growth (Fig. 4). Since the fracture energy behaviour for the two types of material are indistinguishable, the difference in strengths must be due to differences in flaw sizes. The porosity produced by annealing must contribute to a larger effective flaw size. The drastic reduction in strength after annealing at 1750° occurs in material with very large pores and is consistent with this assumption. The strength drop above 1550°C for material hot pressed at 1300°C is more moderate and likely reflects only a drop in fracture toughness.

In summary, the degree of connectivity and distribution of porosity is important in determining its effect on fracture toughness in alumina. For as-hot-pressed material the work-of-fracture results of Coppola and Bradt are confirmed. It is also suggested that surface impurities are an important factor in the determination of fracture toughness of alumina and should be considered in any investigation of microstructural effects.

References

1. P. L. GUTSHALL and G. E. GROSS, *Eng. Frac. Mech.* **1** (1969) 467.
2. A. G. EVANS and G. TAPPIN, *Proc. Brit. Ceram. Soc.* **20** (1972) 275.
3. L. A. SIMPSON, *J. Amer. Ceram. Soc.* **56** (1) (1973) 7.
4. J. A. COPPOLA and R. C. BRADT, *ibid* **56** (7) (1973) 392.
5. H. G. TATTERSALL and G. TAPPIN, *J. Mater. Sci.* **1** (1966) 296.
6. W. F. BROWN and J. E. SRAWLEY, ASTM Special Tech. Pub. No. 410, Philadelphia, 1966.
7. R. C. ROSSI and R. M. FULRATH, US Patent No. 3,343,915, September 26, 1967.
8. *Idem, J. Amer. Ceram. Soc.* **48** (11) (1965) 558.
9. R. W. RICE, US Naval Research Lab. Report 7111, Washington, DC, July 7, 1970.
10. R. W. RICE, *Proc. Brit. Ceram. Soc.* **12** (1969) 99.

Received 21 September
and accepted 20 November 1973

L. A. SIMPSON
G. J. MERRETT
Materials Science Branch,
Atomic Energy of Canada Ltd,
Whiteshell Nuclear Research Establishment,
Pinawa, Manitoba, Canada

The effect of solidification microstructure on the corrosion behaviour of a grain-refined aluminium-copper alloy

The corrosion behaviour of a unidirectionally solidified binary aluminium-4.5 wt % copper alloy in an air-saturated saline environment has recently been investigated [1]. In the solutionized and solutionized-and-aged conditions, grain-boundary attack and intergranular pitting was observed similar to that occurring in corrosion of solutionized wrought alloys [2]. However, in the as-cast condition there was preferential attack of the copper-rich portion of the cored dendritic structure, specifically the α-phase containing more than 3.2 wt % copper. Potential measurements on homogeneous alloys indicated that the α-phase in this range is anodic relative to the θ-phase (Al_2Cu) and to α in the concentration range of 1.6 to 3.2 wt % copper. While α containing less than 1.6 wt % copper also behaves anodically, it did not occur in the examined microstructure of 4.5 wt % copper alloy.

In practice, cast aluminium alloys are grain-refined by innoculation and exhibit an as-cast

microstructure of fine, equiaxed dendritic grains. In order to establish the combined effect of copper and innoculant distributions on the corrosion behaviour of such a material, an aluminium-3.7 wt % copper alloy was grain-refined with addition of 0.11 wt % titanium and studied following the procedure previously described [1]. The alloy was prepared from 99.99 wt % aluminium 99.99 wt % titanium and 99.9 wt % copper; titanium and copper were added as binary master-alloys with aluminium. The ingot was 10 cm × 10 cm × 18 cm and was unidirectionally solidified using a water-cooled stainless steel chill in a preheated mould. Specimens for corrosion and microstructural study were obtained at various distances from the chill in order to incorporate a number of different cooling rates and, hence, of microstructures of different fineness, in this study. Specimens were studied in the as-cast, the solutionized (535°C for 20 h followed by water-quench), and the solutionized-and-aged (155°C for 20 h after the solutionizing treatment) conditions. The corrosive environment employed consisted of a still, air-saturated solution of 3.5 wt % NaCl in distilled water.

The equiaxed dendritic structure of the as-cast alloy is illustrated in Fig. 1. The interdendritic non-equilibrium θ-phase, present as part of a eutectic structure, is clearly visible as is the occurrence of dendrite coring. The distribution of copper, evaluated by electron microprobe analysis along a path AB traversing a typical equiaxed dendrite is shown in the same figure. The path lies entirely within the α-phase. An average 4.6 wt % eutectic was measured next to the chill. This decreased linearly to 3.5 wt % at

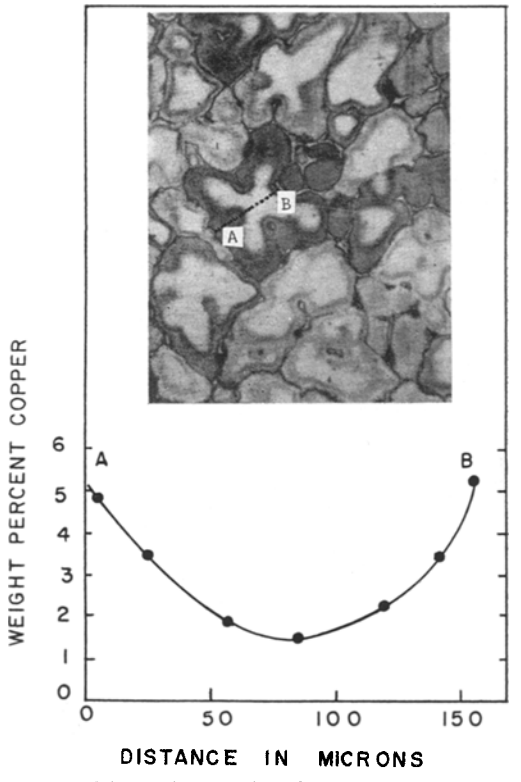

Figure 1 Photomicrograph of the as-cast Al-3.7% Cu-0.11% Ti alloy with copper distribution profile along the shown linear path. Keller's etch, × 120.

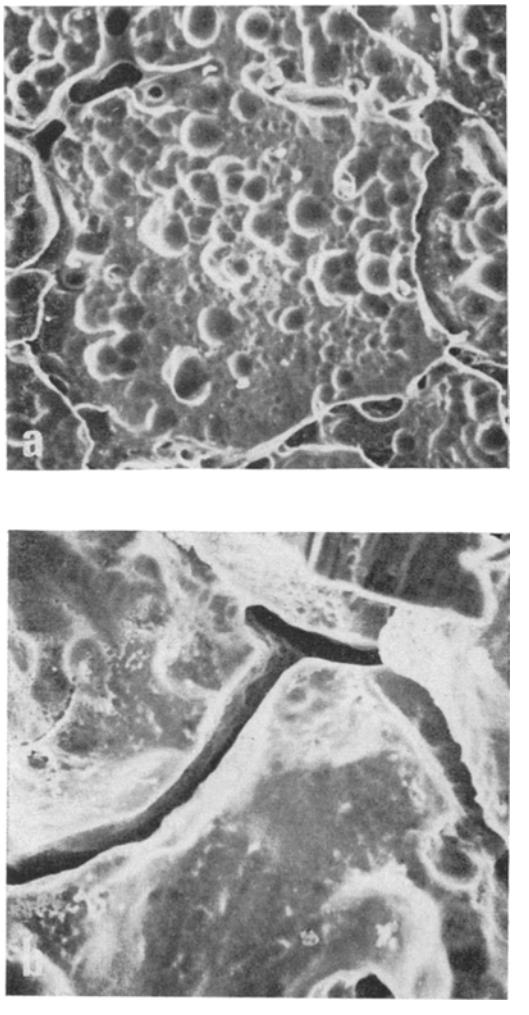

Figure 2 Scanning electron micrograph of the as-cast Al-3.7% Cu-0.11% Ti alloy, corroded for 12 days. (a) × 200, (b) × 500.

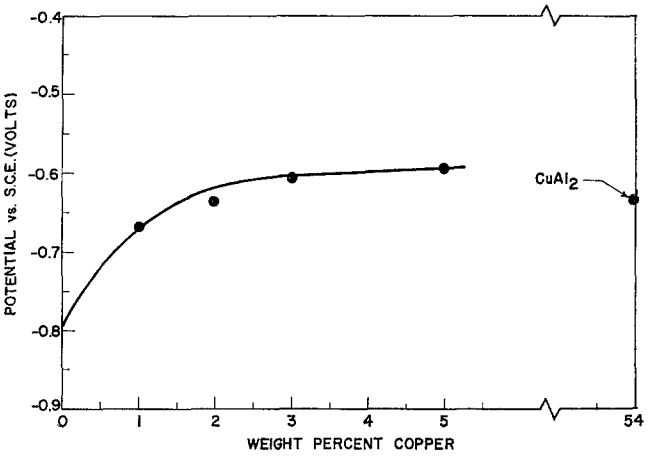

Figure 3 Corrosion potential versus copper concentration for homogeneous ternary Al-Cu-0.11 % Ti alloys.

12 cm from the chill in accord with the reduction in solidification rate [1]. Not all of this microconstituent dissolved during the solutionizing treatment. The residual amount was less next to the chill due to the fine structure accompanying rapid solidification and the corresponding faster solution kinetics. Approximately 0.8 wt % eutectic was measured next to the chill in the solutionized condition. This increased linearly to 1.9 wt % at 12 cm from the chill.

In contrast to observations on the binary columnar alloy [1], corrosion of the as-cast ternary grain-refined alloy was manifested in preferential attack on the non-equilibrium interdendritic eutectic microconstituent and in a less severe, generalized pitting of the α-phase dendrites. Both forms of attack are clearly illustrated in Fig. 2. As in the preceding work [1], potential measurements were made on homogeneous alloys to facilitate the interpretation of microstructural observations. Specimens containing 0.11 wt % titanium and varying amounts of copper were prepared. Potential measurements were made in the test environment using a high resistance electrometer. These data, Fig. 3, indicate that the θ-phase is anodic with respect to the α-phase at copper concentrations greater than about 1.5 wt %, which is the minimum local concentration seen in the cast microstructure. Hence, the severe galvanic attack on the θ-phase is clearly justified. This observation contrasts previously cited observations on the binary columnar alloy. The addition of titanium has made the potential of the θ-phase more negative (active) while raising the potential of the α-phase in the high copper region. This would suggest an effect caused by a non-uniform distribution of titanium between these two phases, as confirmed by electron microprobe analysis.

Behaviour of the solutionized alloy is similar to that of the as-cast material, although the generalized pitting of the α-phase appeared to be on a finer scale. For longer exposure times, however, preferential dissolution on a substructure level is enhanced. These features are shown in Fig. 4 and are attributable to the presence of residual non-equilibrium secondary phase following the solutionizing treatment. Ageing of the solutionized alloy markedly reduces pitting, as shown in Fig. 5. This observation is in agreement with that of Paganelli [3] on wrought binary aluminium-copper alloy.

The effect of cooling and solidification rates, as controlled by the distance from the chill, and hence, of structure fineness, is similar to that in the binary columnar alloy [1]. To obtain an overall evaluation of the extent of corrosion as influenced by this parameter, specimen weight was monitored [1] during exposure to the saline environment. Data are summarized in Fig. 6 showing weight loss as a function of distance from the chill for each of the heat-treatments for both short and long exposures. For the as-cast alloy corrosion decreases with increasing distance from the chill in accord with the parallel decrease in the amount of non-equilibrium secondary phase. In the solutionized, and solutionized-and-aged conditions weight loss may be attributed partly to corrosion of interdendritic non-equilibrium secondary phase and partly to intradendritic pitting corrosion. In these conditions the amount of interdendritic phase increases with

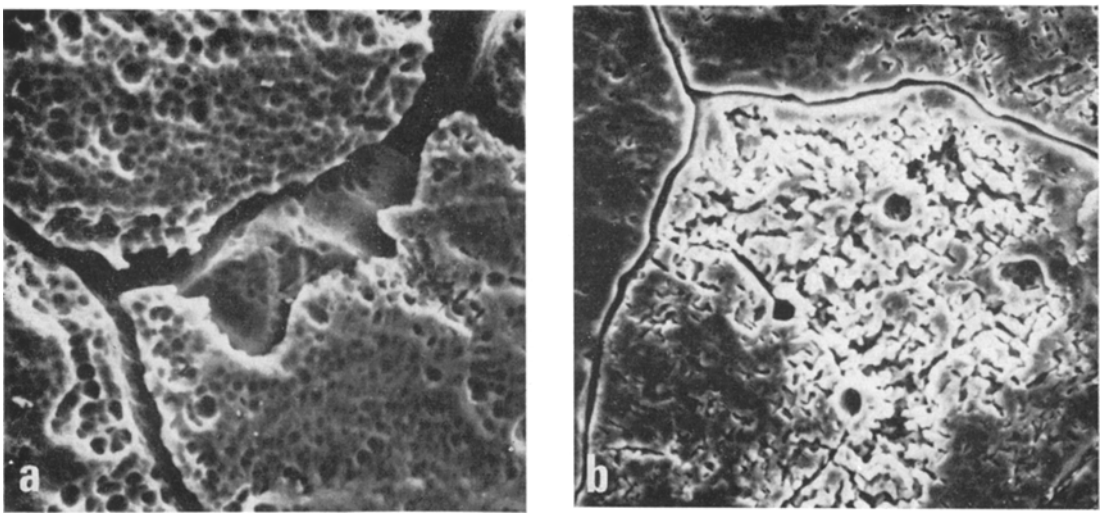

Figure 4 Scanning electron micrographs of the solutionized Al-3.7% Cu-0.11% Ti alloy. (a) Corroded for 12 days, × 550, (b) corroded for 24 days, × 500.

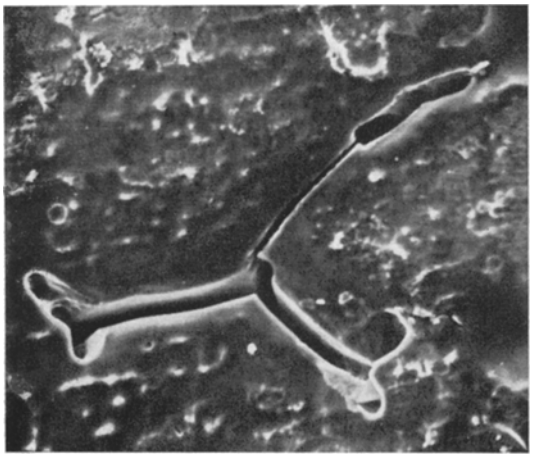

Figure 5 Scanning electron micrograph of the solutionized-and-aged Al-3.7% Cu-0.11% Ti alloy, corroded for 12 days, × 500.

distance from the chill. Pitting corrosion may be attributed to corrosion of precipitated θ-particles within the dendritic α-phase. The amount of this intradendritic phase and, hence, the extent of pitting corrosion, decreases with distance from the chill. The combination of these two corrosion mechanisms can justify the slopes of curves in Fig. 6 for short and long exposure times, if it is assumed that pitting corrosion prevails for shorter exposure times and interdendritic corrosion for longer times.

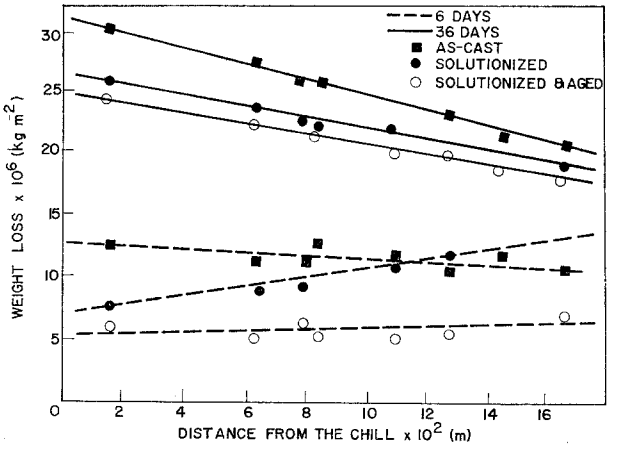

Figure 6 Weight loss for Al-3.7% Cu-0.11% Ti alloy in three heat-treated conditions on exposure to saline solutions versus distance from the chill for representative short and long exposure times.

Acknowledgements

The authors would like to acknowledge the support of the University of Connecticut Research Foundation.

References

1. Y. V. V. R. S. MURTY, T. Z. KATTAMIS, and O. F. DEVEREUX, *Met. Trans.*, **4** (1973) 2575.
2. J. R. GALVELE and S. M. DE DEMICHELI, *Corrosion Sci.* **10** (1970) 795.
3. M. PAGANELLI, *Aluminio* **24** (1955) 335.

Received and accepted
9 November 1973

Y. V. V. R. S. MURTY
T. Z. KATTAMIS
O. F. DEVEREUX
Department of Metallurgy,
Institute of Materials Science,
University of Connecticut,
Storrs, Connecticut, USA

Some observations of glass-ceramic microstructures by cathodoluminescence

The effects of variations of thermal treatment on the microstructures of glass-ceramics prepared by the controlled crystallization of glasses are of interest and, therefore, rapid and convenient methods of characterizing the microstructures are required. The scanning electron microscope (SEM) has become an important tool in the investigation of the surfaces of materials; there are three basic modes in which the SEM can be operated to observe the interactions of an electron beam with the surface of a specimen. These are the electron emission, the X-ray emission and the photon emission from the specimen surface [1].

In this letter we describe some results obtained from observing the cathodoluminescence (CL) or photon emission from a glass-ceramic. The system used to detect the CL consisted of an EMI Type 6255B photomultiplier tube and a 1 in. diameter lens of focal length equal to 1 in. to give a collection angle in excess of 0.75 steradians; a Cambridge Scientific Instruments Ltd, Mk IIA Stereoscan was used.

Two glasses were prepared from compositions shown in Table I; glass A was heat-treated for 2 h at 800°C [2] and glass B was extruded at 825°C. Both glass-ceramics contained needle-shaped crystals of lithium disilicate as their major crystalline phase and a crystalline form of silica as a minor crystalline phase, together with a residual glass phase. Specimens approximately 3 mm thick of each material were polished to 1 μm and coated with a layer approximately 10 nm thick of gold/palladium to prevent charging in the SEM. The polished surfaces were examined in the SEM by the secondary emission mode and the CL mode. The accelerating potential was 30 kV, the beam current approximately 150 μA and the specimen was positioned normal to the incident electron beam.

TABLE I Glass compositions in mol%.

	SiO_2	Li_2O	K_2O	Al_2O_3	P_2O_5	B_2O_3
Glass A	61.0	30.5	1.5	1.0	1.0	5.0
Glass B	67.5	24.0	1.5	1.0	1.0	5.0

Figs. 1 and 2 show a comparison of the same area of glass A observed in the two modes; Fig. 3 shows a sample prepared in the same fashion but etched for 30 sec in a 3% HF solution and observed in the secondary/reflected mode. There is obviously a marked contrast mechanism in the CL mode which enables the lithium disilicate crystalline phase to be easily distinguished from the glassy matrix; the CL micrograph has a speckled appearance because of noise associated with the photomultiplier.

Figs. 4 and 5 show a similar comparison in glass B. A weak contrast mechanism can be observed in the secondary/reflected emission micrograph which is caused by the back-scattered electrons [3]; the darker crystalline regions in Fig. 4 show little electron emission but a strong photon emission in Fig. 5. Prior etching of the glass-ceramic, in the manner described above, enabled the micrograph shown in Fig. 6 to be obtained by the secondary/reflected mode.

CL has been observed in quartz [4] but in the present studies no CL was observed from the silica crystalline phase; one of the emission bands in quartz [5] is positioned outside the range of the photomultiplier tube used and the strong emission from the disilicate phase together with the small volume fraction of the silica crystals makes detection of the CL of the latter difficult.